



**HAL**  
open science

# Liquid-assisted vapor-solid-solid silicon nanowire growth mechanism revealed by in situ TEM when using Cu-Sn bimetallic catalysts

Eric Ngo, Weixi Wang, Pavel Bulkin, Ileana Florea, Martin Foldyna, Pere Roca I Cabarrocas, Jean-Luc Maurice

## ► To cite this version:

Eric Ngo, Weixi Wang, Pavel Bulkin, Ileana Florea, Martin Foldyna, et al.. Liquid-assisted vapor-solid-solid silicon nanowire growth mechanism revealed by in situ TEM when using Cu-Sn bimetallic catalysts. *Journal of Physical Chemistry C*, 2021, 10.1021/acs.jpcc.1c05402 . hal-03323825

**HAL Id: hal-03323825**

**<https://hal.science/hal-03323825>**

Submitted on 23 Aug 2021

**HAL** is a multi-disciplinary open access archive for the deposit and dissemination of scientific research documents, whether they are published or not. The documents may come from teaching and research institutions in France or abroad, or from public or private research centers.

L'archive ouverte pluridisciplinaire **HAL**, est destinée au dépôt et à la diffusion de documents scientifiques de niveau recherche, publiés ou non, émanant des établissements d'enseignement et de recherche français ou étrangers, des laboratoires publics ou privés.

# Liquid-assisted vapor-solid-solid silicon nanowire growth mechanism revealed by *in situ* TEM when using Cu-Sn bimetallic catalysts

*Eric Ngo, Weixi Wang, Pavel Bulkin, Ileana Florea, Martin Foldyna, Pere Roca i Cabarrocas and Jean-Luc Maurice\**

LPICM, École polytechnique, CNRS UMR7647, Institut Polytechnique de Paris, 91120 Palaiseau, France

KEYWORDS. Silicon nanowires, VLS/VSS, bimetallic catalysts, dual-phase catalysts, *in situ* TEM.

## ABSTRACT

The vapor-liquid-solid (VLS) and vapor-solid-solid (VSS) growth mechanisms are widely used to obtain silicon nanowires. In this paper, we report on a hybrid method based on the use of a dual-phase catalyst made of liquid Sn and solid Cu<sub>3</sub>Si, which results in a liquid-assisted VSS (LA-VSS) mechanism. The silicon atoms are brought by atomic hydrogen-assisted dissociation of silane molecules. We observe the growth *in situ*, in the transmission electron microscope, at

atomic resolution. We show that the dual-phase catalyst favors the  $\langle 111 \rangle$  crystallographic orientation. Each new Si (111) plane nucleates at the interface between the liquid and solid parts of the catalyst before propagating rapidly along the interface of Si top facet with the liquid part, and slowly along the interface with the solid part. Moreover, we show that structural properties of the Si nanowires, such as the growth direction and the twin density, can be controlled by adjusting the Sn/Cu ratio.

## 1. Introduction

Silicon nanowires (SiNWs) are building blocks for a variety of electronic and optoelectronic devices (1-5) and for biological (6, 7) and chemical sensors. (8) They can also be used as anodes for portable energy storage applications. (9) The vapor-liquid-solid (10) (VLS) or the vapor-solid-solid (11) (VSS) techniques are the most widely used for growing SiNWs. They require metallic particles, either in a liquid or solid form, to catalyze the dissociation of silicon precursors and incorporate silicon atoms until reaching supersaturation, which triggers the precipitation of a crystalline NW. Several metallic elements were found to effectively grow SiNWs. The VLS mechanism with an Au-based eutectic as catalyst, for the growth of  $\langle 111 \rangle$  oriented semiconductor NWs, is particularly well documented, (12) noticeably thanks to *in situ* transmission electron microscopy (TEM) observations. (13-16) The VSS mechanism with  $\text{Cu}_3\text{Si}$  as catalyst has also been the object of a detailed analysis. (17) Metal alloys such as AuAg, (18) AuCu, (19) AuGa (20) and BiSn have been used as well and have proved to be efficient catalysts. (21) However, how SiNWs grow when the catalyst is made of a mixture of metals remains an open question. In the present work, we performed SiNW growth *in situ* in an atomic-resolution TEM, using Cu-Sn bimetallic catalysts. Our observations uncover a specific growth mechanism that implies liquid and solid phases together, making up a combined VLS/VSS

technique that we call liquid-assisted VSS (LA-VSS). The two metals, Cu and Sn, were chosen as they are thought to facilitate the formation of the metastable hexagonal-diamond structure in SiNWs (22, 23). Our study of the nucleation of that metastable phase is the object of a forthcoming paper.

## 2. Results and discussions

Prior to nanowire growth, the catalyst particles are annealed *in situ* at 250°C in an atomic-H atmosphere, so that their oxides be reduced and their shapes stabilized. The catalyst particle size distribution changes during this process, see Video 1, Figure S1 in the Supporting Information and refs. (23, 24). In absence of Cu, liquid Sn particles tend to coalesce (see Figure S1a-b), while with Cu (melting point  $T_m = 1085$  °C), liquid Sn ( $T_m = 232$  °C) sticks to solid Cu particles (Figure S1e-f), which offers the interesting possibility of narrowing the SiNW diameter distribution. (23)

### 2.1. Structural and compositional analysis of dual-phase catalysts during NW growth

**Figure 1** displays SiNWs obtained with a catalyst nominal Sn/Cu atomic ratio of 52/48. **Figure 1a** clearly shows that the catalytic seed on a  $\langle 111 \rangle$  SiNW growing at 500 °C presents at the same time a solid phase, evidenced by the faceted structure and the lattice fringes, and a liquid phase forming a spherical droplet. To examine the chemical composition of the two phases, we performed energy-dispersive X-ray spectroscopy (EDX) on the SiNW shown in **Figure 1b**. In this nanowire, the left part is faceted and thus solid; while the right part displays a spherical shape characteristic of a liquid droplet. Spectrum L in **Figure 1c** was recorded with a stationary beam on the liquid part while S was obtained with the beam on the solid part. The liquid part is Sn-rich with a composition of 63 at. % Sn and 37 at. % Cu, if we exclude Si from

the total count. Conversely, the solid part is Cu-rich with 16 at. % Sn and 84 at. % Cu, excluding Si again. Given the influence of the other phase in each spectrum (due to backscattered electrons), this analysis shows a neat separation between a crystalline Cu-rich part and a liquid

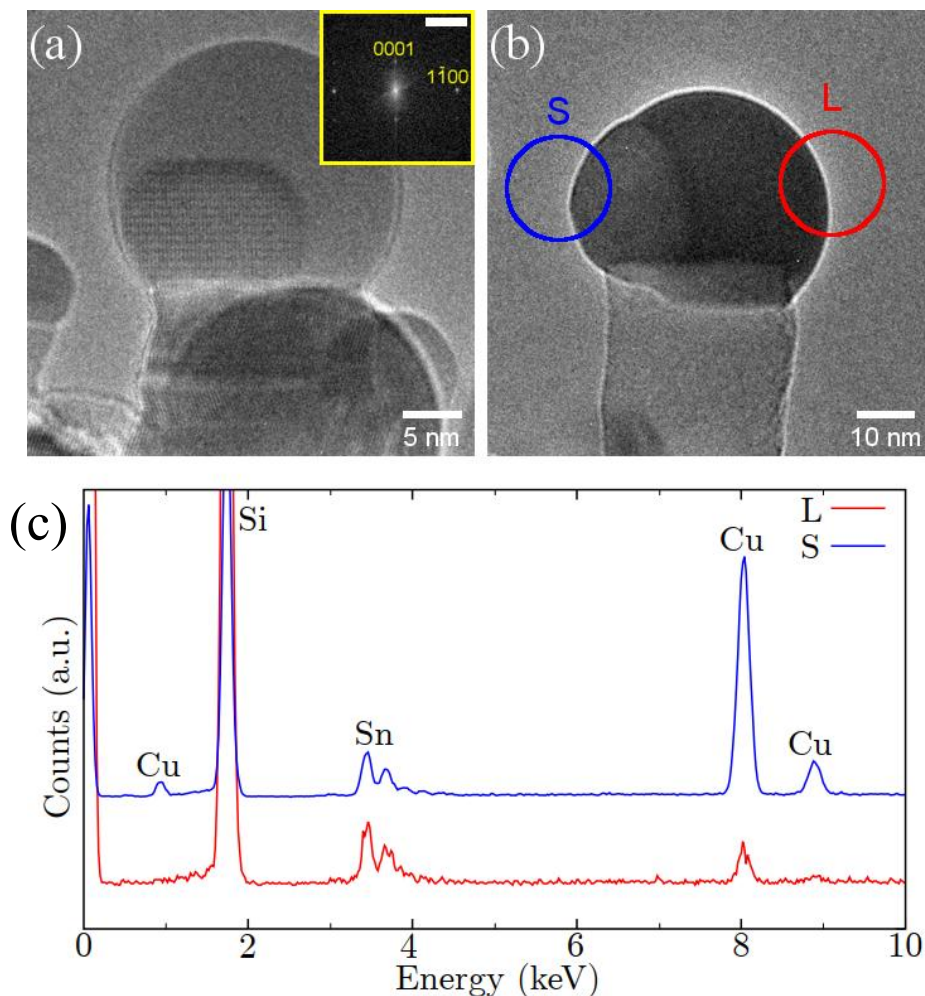


**Figure 1.** Chemical characterization of a Cu-Sn catalyst on a SiNW. a) TEM micrograph of a Cu-Sn catalyst where a crystalline and a liquid part are visible. Inset: fast Fourier transform of the solid part. Scale:  $2 \text{ nm}^{-1}$ . b) Cu-Sn catalyst where the EDX measurements are carried out, where a separation between a faceted solid and a liquid spherical droplet is again visible. c) EDX spectra of the catalyst taken in the liquid (L) and solid (S) regions.

Sn-rich region with some Si in both parts. The difference of phase can be explained by the difference in melting points between the two metals or compounds [see the Cu-Sn phase diagram (25)].

We have shown that the crystalline part contains mostly Cu. However, we have not yet considered the presence of Si: if the Si peak in **Figure 1c** essentially comes from the NW itself, some of it also comes from the catalyst. More information on the nature of this crystal can be gathered through electron diffraction, see **Figure 2a**. Comparing the experimental diffraction patterns to simulations performed with the JEMS package (26, 27) allows us to characterize the

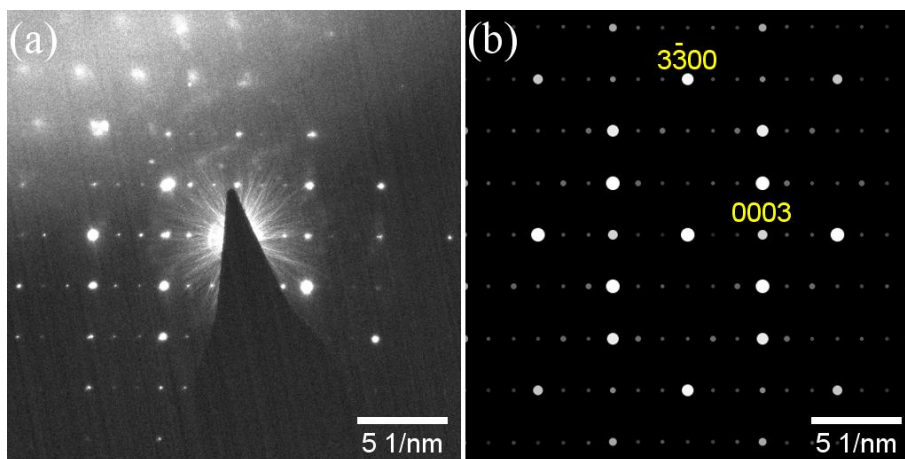


**Figure 2.** Structural characterization of the solid Cu-rich part of a Cu-Sn catalyst on top of a SiNW. a) Experimental electron diffraction pattern. b) Simulated electron diffraction pattern of the  $\eta$ -Cu<sub>3</sub>Si compound along the  $[11\bar{2}0]$  zone axis.

Cu-rich crystal structure. We find that the best fit to the experimental data is for the copper silicide  $\eta$ -Cu<sub>3</sub>Si (28), with space group  $P\bar{3}m1$  and lattice parameters  $a = 4.06 \text{ \AA}$  and  $c = 7.33 \text{ \AA}$ : the two patterns coincide in both the pattern and the distance between spots. The result of the simulation along the  $[11\bar{2}0]$  zone axis is shown in **Figure 2b**. Quite interestingly, this compound

was also that found by the authors that had studied pure-Cu catalyzed VSS growth of SiNWs at higher temperatures. (29-32)

SiNWs obtained from an initial Sn/Cu deposit with a total nominal thickness of 0.7 nm have a diameter that ranges from 5 nm to 30 nm. We find that the dual-phase structure of the catalyst occurs along the whole range of obtained diameters. For example, **Figure 3** shows a SiNW with a diameter of 6.1 nm at the top where a solid  $\text{Cu}_3\text{Si}$  phase with a lateral width of 4 nm coexists with a pocket of liquid. There seems to exist a critical size at around 3 nm for the solid  $\text{Cu}_3\text{Si}$  to remain at the top though. Below this size, the solid  $\text{Cu}_3\text{Si}$  rapidly vanishes under irradiation by the electron beam, leaving only the Sn-rich liquid (see Video 2). The depletion of the Cu-rich catalyst is most likely due to the diffusion of Cu towards the substrate through the NW as indeed, Cu is known to be a fast diffuser in Si. (33, 34) The incident electron beam can trigger this out-of-catalyst diffusion by cracking both the Cu-Cu and Cu-Si chemical bonds in the catalysts. The examination of the fast Fourier transform (FFT) on the solid catalyst in **Figure 1a** reveals that the top and bottom surfaces of the Cu catalyst are actually (0001) surfaces. The solid  $\text{Cu}_3\text{Si}$  and the SiNW are then in a  $(111)_{\text{Si}}/(0001)_{\text{Cu}_3\text{Si}}$  epitaxial relationship, which explains an observed preference for the growth of  $\langle 111 \rangle$  oriented SiNWs.

Interestingly, the Sn-rich liquid and the solid  $\text{Cu}_3\text{Si}$  are both in contact with the nanowire in a large majority of the observed SiNWs (one exception found in over hundred observed NWs), no matter the size of each respective part and the diameter of the nanowire. Consequently, both parts play a role during the growth of SiNWs.

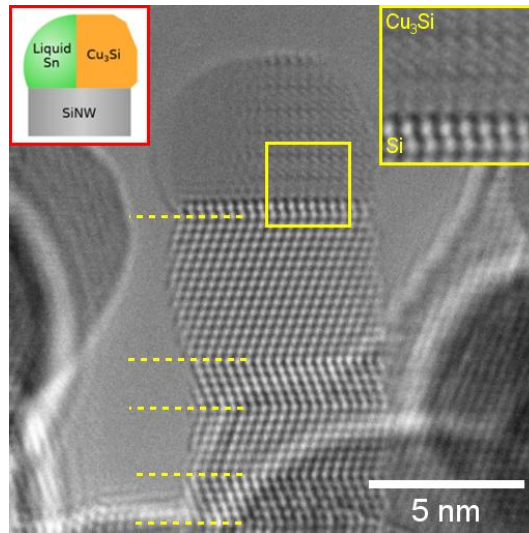


**Figure 3.** Demonstration of the dual-phase nature of Cu-Sn catalysts on top of a very small diameter  $\langle 111 \rangle$ -SiNW grown at 500 °C. The solid  $\text{Cu}_3\text{Si}$  part (on the right) is clearly identifiable thanks to its faceting and the presence of lattice fringes. The yellow dotted lines indicate twin planes in the SiNW. Inset: close-up view of the yellow squared area, demonstrating the  $(111)_{\text{Si}}/(0001)_{\text{Cu}_3\text{Si}}$  epitaxial relationship between the SiNW and  $\text{Cu}_3\text{Si}$ .

## 2.2. Step-flow kinetics during growth with dual-phase catalysts

To unravel the growth mechanisms with a dual-phase catalyst, we have selected a SiNW and recorded its evolution during the growth. This nanowire, shown in **Figure 4**, is  $[111]$  oriented and has a diameter of 15 nm. The catalyst-nanowire interface is planar in our SiNWs, which is in contrast with NWs grown with more common Au-Si eutectic alloy catalyst, which usually present a truncated edge close to the triple-phase line. (35) **Figure 4a-c** shows the formation of a  $(111)$  atomic plane. Firstly, six seconds after recording has started (see Video 3), this plane

appears at the catalyst-nanowire interface inside the Sn-rich liquid. The nucleation of a new layer thus begins on the liquid side. This can be related to the low Si solubility in liquid Sn (36) compared to solid Cu or  $\text{Cu}_3\text{Si}$ . (37) The low solubility ensures that a high Si supersaturation is reached quickly, overcoming the Si nucleation barrier. The expansion of this first layer to the  $\text{Cu}_3\text{Si}$  solid part starts after a waiting time of four seconds, probably due to the higher Si solubility in that compound, which shifts supersaturation towards high Si-concentration. Four seconds later, another single (111) layer is created on the Sn side so that it results in a two-atomic plane-high step waiting at the liquid Sn-solid  $\text{Cu}_3\text{Si}$  interface, see **Figure 4b**. Following this, a single Si (111) plane starts extending laterally under the solid Cu-rich part at a much slower rate than in the liquid as shown by the yellow arrows in **Figure 4c**. It is only 10 seconds after that, that the second layer starts extending as well. Thus, like in VLS and VSS, growth with our bimetallic catalyst occurs in a step-flow fashion. (11, 18, 32, 38)

Additional information can be retrieved by observing the nanowire over the course of the growth of several monolayers. During the 160-second recording (see Video 3), seven Si (111) planes were formed. We have tracked the time evolution of the step edges positions of the two first growing planes in **Figure 4e** (more data in Figure S1). A position at 0 means that the new plane has not yet formed while that same plane is fully completed if the position is 1. An intermediate value denotes that the new plane only covers part of the SiNW, see **Figure 4d**. From **Figure 4e**, we see that the two planes are growing at the same time. The curves are vertical between positions 0 and  $\sim 0.45$  (Sn- $\text{Cu}_3\text{Si}$  interface) because the recording time of the camera (0.25 s per frame) does not allow to discriminate those two points. The difference in propagation velocities between liquid Sn and solid  $\text{Cu}_3\text{Si}$  is thus immediately visible, which is the consequence of the difference in Si incorporation rate as discussed above. Single plane

growth is the norm in the liquid Sn, while  $\text{Cu}_3\text{Si}$  favors a growth that often occurs with two planes at a time. Such a phenomenon can be attributed to the slow Si diffusion rate inside a solid

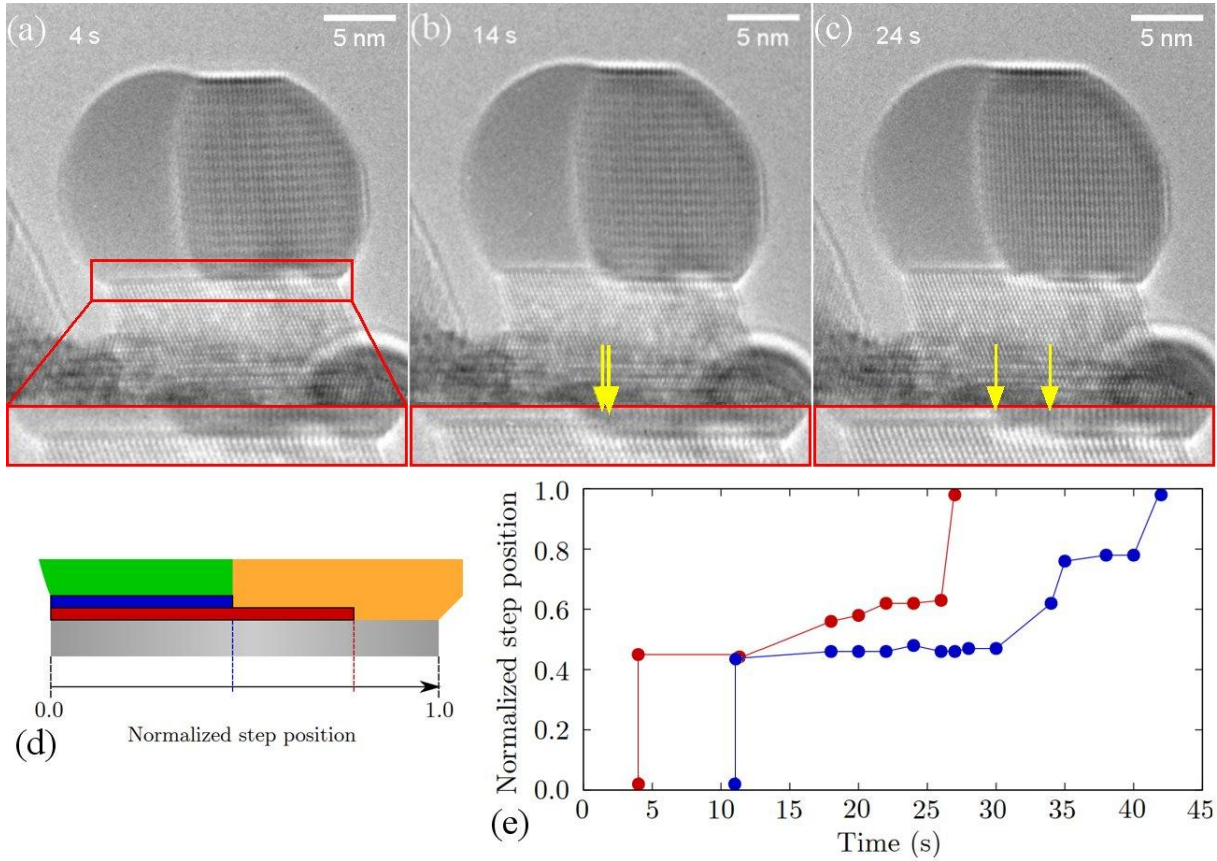


**Figure 4.** Step-flow mechanism in Cu-Sn catalysts. a)-c) Snapshots of two growing (111) planes. The yellow arrows indicate the positions of the two steps. A zoom of the SiNW-catalyst interface is presented at the bottom of each figure. d) Schematic depicting how the positions of the two plane steps are calculated in e); the grey part is the SiNW, the green part is the Sn-rich liquid and the orange part is the solid  $\text{Cu}_3\text{Si}$ ; the blue and red rectangle represent the two growing Si (111) planes in a)-c). e) Normalized step position evolution for the two growing planes in a)-c).

catalyst. (39) Another notable feature of the step edge position is the bi-periodic nature of the nucleation on the Sn side (Figure S1). We see that every two nucleation events in the liquid Sn, the process is generally followed by a longer waiting time. One would expect instead that nucleation would occur at a fixed rate because of a constant arrival rate of Si precursor in the catalyst: in the Cu-catalyzed growth of SiNWs by VSS, this is indeed the case; (39) in the VLS growth of NWs with pure Sn, it is also the case (see our *in situ* recording, Figure S2). But here, the overall kinetics is limited by the relatively slow solid-state diffusion of Si atoms in the  $\text{Cu}_3\text{Si}$  crystal. Thus, the growth of Si (111) steps on the  $\text{Cu}_3\text{Si}$  side creates a Si-atom depletion that translates itself into significant Si concentration gradients in  $\text{Cu}_3\text{Si}$ , not only between the external surfaces of the catalyst and its interface with the SiNW, but also between the boundary with the Sn-rich part and that interface, resulting in a net flow of Si atoms from the liquid Sn-rich part towards the solid  $\text{Cu}_3\text{Si}$ . This leak, towards  $\text{Cu}_3\text{Si}$ , would act in turn as a retardant for the nucleation of new Si (111) steps on the liquid side.

At the frame rate of the camera used for Video 3 and **Figure 4** (four frames per second – fps), the nucleation site of Si (111) steps could not be localized. We thus used a faster camera also available on the microscope, to determine the nucleation place of that step, see Video 4 and **Figure 5**. Nucleation takes place at the liquid Sn(Cu)- $\text{Cu}_3\text{Si}$ -Si triple line, most probably at the quadruple point defined by that line and the perimeter of the interface between catalyst and NW. A part of the nucleus appears to be on the  $\text{Cu}_3\text{Si}$  side (**Figure 5c**); it is probably an effect of projection, as the  $\text{Cu}_3\text{Si}$ -Sn(Cu) boundary is neither flat nor parallel to the beam. The new Si monolayer invades the interface with the liquid part of the catalyst in approximately 0.05s.

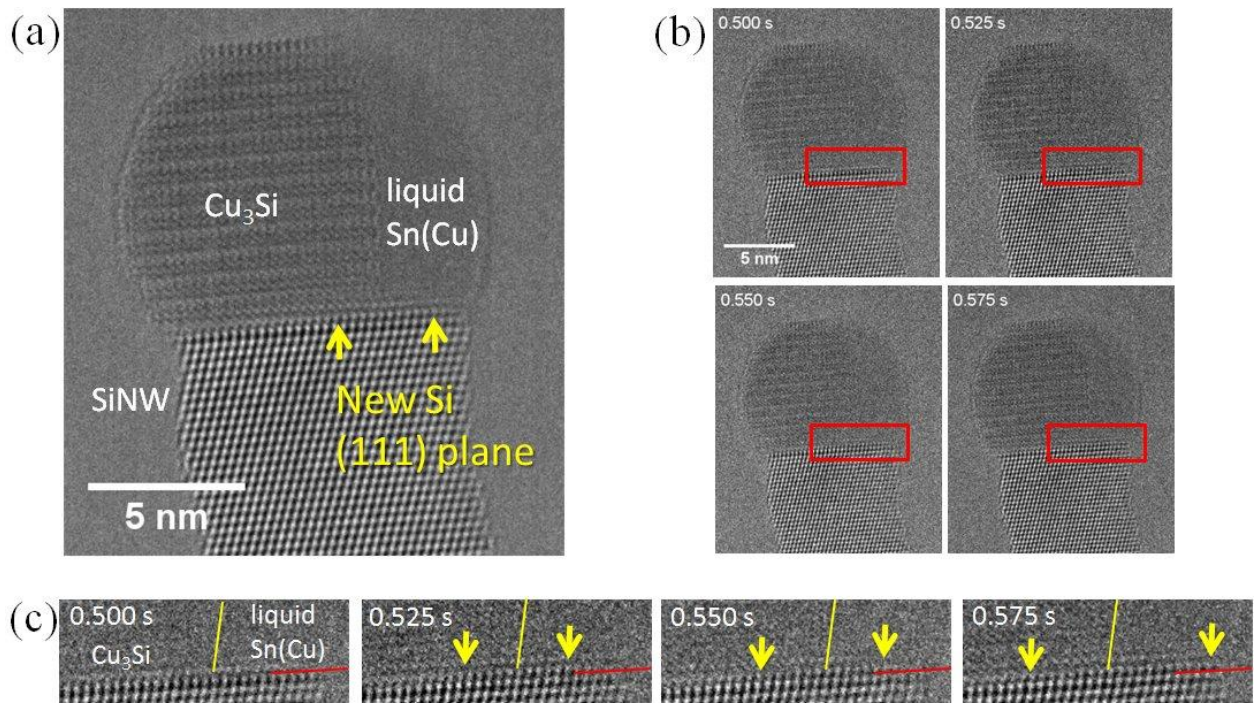


**Figure 5.** TEM images taken from Video 4, recorded at a rate of 40 fps, with time origin taken at the beginning of Video 4. The yellow arrows show the two edges of a new Si (111) plane, absent at  $t = 0.500$  s. a) Image centred on frame 0.525 s, averaged over seven frames (0.2 s integrated exposure time) so that the boundary between  $\text{Cu}_3\text{Si}$  and liquid  $\text{Sn}(\text{Cu})$  be visible. b) Four non-averaged frames where the new (111) Si monolayer nucleates. c) Enlargements of the areas squared in (b); the yellow line indicates the position of the  $\text{Cu}_3\text{Si}$ - $\text{Sn}(\text{Cu})$  boundary, the red one shows the initial position of the catalyst-Si interface.

### 2.3. Catalyst evolution upon cooling

As standard characterization of NWs is performed *ex situ*, after growth, we have followed the evolution of catalyst structure during the cooling of the specimen to check possible changes during this part of the treatment. Quite interestingly, a new phase nucleates in the liquid part,

made of hexagonal  $\eta$ -Cu<sub>6</sub>Sn<sub>5</sub>, see Video 5 and Figure S2. Thus, a post-growth characterization could conclude on the presence of that phase during growth, and give it a role in the growth, while it has only appeared upon cooling.

#### **2.4. Catalysts combination for a fine control of SiNW features**

Let us now consider the features of SiNWs catalyzed by both Cu and Sn and their changes as a function of the Sn/Cu ratio. Figure S7 shows that on a Si flat (111) surface, the majority of the SiNWs are straight and mainly grow epitaxially along the [111] direction. Some nanowires present a quasiperiodic (111) twinning perpendicular to the growth axis (**Figure 3**) while others have no defects at all. Analyzing the catalysts on top of these wires, the determining factor for twinning to occur appears to be the ratio of Sn/Cu: a ratio in favor of liquid Sn will inhibit the formation of twin planes. In contrast, growth with only solid Cu<sub>3</sub>Si even on a Si (111) surface, mostly yields  $\langle 112 \rangle$  wires with twin planes parallel to the nanowire axis (Figure S5). The change in the growth direction is linked to a modification in the Cu<sub>3</sub>Si particle orientation with respect to the Si (111) surface before the NW growth when some of its facets are wetted by liquid Sn (Figure S6). Bare Cu<sub>3</sub>Si particles are in contact with the Si (111) surface via their bottom (10 $\bar{1}$ 0) facets while Sn-wetted Cu<sub>3</sub>Si do so with their (0001) facets. Thus, adding Sn to Cu allows one to change the NW growth direction from  $\langle 112 \rangle$  to  $\langle 111 \rangle$  and, on the high-Sn content side, to obtain single crystals NWs instead of multiply twinned ones.

Through *in situ* observation, we arrive at the conclusion that, by controlling the deposited Sn/Cu ratio, it is possible to *i*) select the growth direction, *ii*) control presence of twins and *iii*) tune the diameter and straightness of the grown wires. Catalysts mixing and feature selection through control of the deposited ratio should be applicable to other binary catalysts with very

different Si solubility and melting points. For example, we expect that substituting Sn with In to form Cu-In catalysts should also give dual-phase catalysts and tunable nanowires features. As more than ten different metals are known to catalyze nanowire growth, (40) other substitutions could prove fruitful in modifying structures such as stabilizing exotic Si polytypes. Therefore, we believe that double-catalyst assisted growth constitutes a promising direction to obtain SiNWs with a diverse set of properties.

### **3. Conclusion**

We have presented a liquid-assisted vapor-solid-solid (LA-VSS) mechanism to grow silicon nanowires based on the use of bimetallic Cu-Sn nanoparticles. We have shown that Cu-Sn catalysts are dual-phase during NW growth with a distinct Sn-rich liquid part and a solid  $\eta$ -Cu<sub>3</sub>Si part. The *in situ* TEM analysis of the growth process reveals that during the growth of <111> oriented wires, both phases work together to produce each new Si (111) plane. In this LA-VSS process an atomic step first appears in liquid Sn and waits for a second (111) plane to join before crossing the Sn-Cu<sub>3</sub>Si interface. Expansion resumes once there is a sufficient amount of available Si in the solid catalyst. In this configuration, the liquid catalyst part delivers Si atoms to the solid catalyst part, to give a constant growth rate. Adjusting the deposited Cu/Sn ratio, it is possible to control the diameter, the growth direction, and the presence or not of twins in the Si NWs (23). Such precise control has not been possible before with single metal catalyst nanoparticles. We expect this approach to open the way to a broader range of applications.

### **4. Experimental Section/Methods**

Silicon NWs were grown through hydrogen atom-assisted chemical vapor deposition (CVD) in a modified Thermo Fisher Titan environmental transmission electron microscope (ETEM)

“NanoMAX”, using bimetallic catalysts consisting of Cu and Sn. Catalysts were obtained from the sequential thermal evaporation in a Boc Edwards Auto 306 Evaporator FL 400, at a pressure of  $10^{-5}$  mbar, of Cu first and Sn in a second run. The tested atomic Sn/Cu ratios were 37/63 and 52/48. The total evaporated metal thickness, measured by a quartz microbalance, did not exceed 0.7 nm. The Cu-Sn particles were deposited on two different types of substrate: a Protochips Fusion SiC membrane and a (110) Si wafer cut in a cantilever geometry so that the SiNWs grow perpendicular to the electron beam, epitaxially on a (1 $\bar{1}$ 1) Si surface, enabling easier observations along the [110] zone axis and give access to atomic resolution. (41, 42) These Si cantilever substrates were exposed to 40 % HF vapor for 4 minutes to remove the native oxide. Substrate heating was done by running an electrical current in either the SiC membrane or the cantilever. A gas mixture of 3/97 SiH<sub>4</sub>/H<sub>2</sub> (volume ratio) was used to grow the SiNWs so that the total pressure inside the TEM column was in the  $10^{-2}$  mbar range. Atomic hydrogen was produced remotely from H<sub>2</sub> gas thanks to an ECR plasma source (Aura-wave from SAIREM) functioning at a micro-wave frequency of 2.45 GHz and operating at a power of 50 W. The way from the plasma source to the sample was straight, about 30-cm long with a smallest diameter of 2 cm. After introducing samples with the evaporated Cu-Sn particles in the ETEM, an annealing at 250 °C for 10 minutes under a flux of hydrogen atoms was carried out. The temperature was then further increased to 380 °C or more at which point the SiH<sub>4</sub> gas was introduced at the above ratio. SiNWs were observed to grow at a rate of the order of  $0.015 \text{ nm}\cdot\text{s}^{-1}$ . The method is thus a radical-assisted chemical vapor deposition (RA-CVD). An incubation time of up to one hour was observed, due to the time taken for the Cu<sub>3</sub>Si compound to form because of low Si diffusion rate in Cu. The cameras used included a US1000, working at a frequency of four fps, and a K2IS, working at a frequency of 400 fps, averaged to 40 fps, both from Gatan.

**Supporting Information.** The following files are available free of charge.

- Supporting information file, giving explanations of videos and seven additional figures (MS Word)

- Videos 1 to 5 (AVI).

### **Corresponding Author**

\*jean-luc.maurice@polytechnique.edu.

### **Author Contributions**

ÉN carried out the investigations, helped by JLM, IF & WW; ÉN analyzed the data; PB designed and implemented the *in situ* atomic-hydrogen delivery system; JLM, PRC & MF acquired the Funding; JLM administrated the project; JLM, MF & PRC supervised the work; ÉN wrote the first draft of the paper, JLM, MF & PRC wrote the final version. All authors have given approval to the final version of the manuscript.

### **Funding Sources**

This research was funded by the French National Research Agency, ANR, through the TEMPOS Equipex, pole NanoMAX, grant number ANR-10-EQPX-50, and the HexaNW project, grant number ANR-17-CE09-0011.

### **Acknowledgements**

We kindly thank Federico Panciera for providing the cantilever substrates, and Frank Glass (both at Université Paris-Saclay, CNRS, C2N) for fruitful discussions. Thanks are also due to the CIMEX – Centre interdisciplinaire de microscopie électronique de l’X, for the use of the electron microscopes at École polytechnique.

## ABBREVIATIONS

TEM, transmission electron microscopy; ETEM, environmental TEM; CVD, chemical vapor deposition; RA-CVD, radical-assisted CVD; ECR, electron cyclotron resonance; VLS, vapor-liquid-solid; VSS, vapor-solid-solid; LA-VSS; liquid-assisted VSS.

## REFERENCES

1. Li, Y.; Qian, F.; Xiang, J.; Lieber, C. M. Nanowire electronic and optoelectronic devices. *Materials Today* 2006, 9, (10), 18-27, DOI: 10.1016/S1369-7021(06)71650-9
2. Jia, C.; Lin, Z.; Huang, Y.; Duan, X. Nanowire Electronics: From Nanoscale to Macroscale. *Chem. Rev.* 2019, 119, (15), 9074-9135, DOI: 10.1021/acs.chemrev.9b00164
3. Chen, W.; Roca i Cabarrocas, P. Rational design of nanowire solar cells: from single nanowire to nanowire arrays. *Nanotechnology* 2019, 30, (19), 194002, DOI: 10.1088/1361-6528/aaff8d
4. Misra, S.; Yu, L.; Chen, W.; Foldyna, M.; Roca i Cabarrocas, P. A review on plasma-assisted VLS synthesis of silicon nanowires and radial junction solar cells. *J. Phys. D: Appl. Phys.* 2014, 47, (39), 393001, DOI: 10.1088/0022-3727/47/39/393001
5. Zhang, T.; Wang, J.; Yu, L.; Xu, J.; Roca i Cabarrocas, P. Advanced radial junction thin film photovoltaics and detectors built on standing silicon nanowires. *Nanotechnology* 2019, 30, (30), 302001, DOI: 10.1088/1361-6528/ab0e57
6. Cui, Y.; Wei, Q.; Park, H.; Lieber, C. M. Nanowire Nanosensors for Highly Sensitive and Selective Detection of Biological and Chemical Species. *Science* 2001, 293, (5533), 1289-1292, DOI: 10.1126/science.1062711
7. Gao, A.; Lu, N.; Wang, Y.; Dai, P.; Li, T.; Gao, X.; Wang, Y.; Fan, C. Enhanced Sensing of Nucleic Acids with Silicon Nanowire Field Effect Transistor Biosensors. *Nano. Lett.* 2012, 12, (10), 5262-5268, DOI: 10.1021/nl302476h
8. Luo, L.; Jie, J.; Zhang, W.; He, Z.; Wang, J.; Yuan, G.; Zhang, W.; Wu, L. C. M.; Lee, S.-T. Silicon nanowire sensors for Hg<sup>2+</sup> and Cd<sup>2+</sup> ions. *Appl. Phys. Lett.* 2009, 94, (19), 193101, DOI: 10.1063/1.3120281
9. Zamfir, M. R.; Nguyen, H. T.; Moyen, E.; Lee, Y. H.; Pribat, D. Silicon nanowires for Li-based battery anodes: a review. *J. Mater. Chem. A* 2013, 1, (34), 9566-9586, DOI: 10.1039/C3TA11714F
10. Wagner, R. S.; Ellis, W. C. Vapor-liquid-solid mechanism of single crystal growth. *Appl. Phys. Lett.* 1964, 4, (5), 89-90, DOI: 10.1063/1.1753975

11. Wen, C. Y.; Reuter, M. C.; Bruley, J.; Tersoff, J.; Kodambaka, S.; Stach, E. A.; Ross, F. M. Formation of Compositionally Abrupt Axial Heterojunctions in Silicon-Germanium Nanowires. *Science* 2009, 326, (5957), 1247-1250, DOI: 10.1126/science.1178606
12. Dubrovskii, V. G.; Sibirev, N. V.; Harmand, J. C.; Glas, F. Growth kinetics and crystal structure of semiconductor nanowires. *Phys. Rev. B* 2008, 78, (23), 235301, DOI: 10.1103/PhysRevB.78.235301
13. Ross, F. M.; Tersoff, J.; Reuter, M. C. Sawtooth faceting in silicon nanowires. *Phys. Rev. Lett.* 2005, 95, (14), 146104,
14. Hannon, J. B.; Kodambaka, S.; Ross, F. M.; Tromp, R. M. The influence of the surface migration of gold on the growth of silicon nanowires. *Nature* 2006, 440, (7080), 69-71,
15. Gamalski, A. D.; Tersoff, J.; Stach, E. A. Atomic Resolution in Situ Imaging of a Double-Bilayer Multistep Growth Mode in Gallium Nitride Nanowires. *Nano. Lett.* 2016, 16, (4), 2283-2288, DOI: 10.1021/acs.nanolett.5b04650
16. Harmand, J.-C.; Patriarche, G.; Glas, F.; Panciera, F.; Florea, I.; Maurice, J.-L.; Travers, L.; Ollivier, Y. Atomic Step Flow on a Nanofacet. *Phys. Rev. Lett.* 2018, 121, (16), 166101, DOI: 10.1103/PhysRevLett.121.166101
17. Wen, C. Y.; Tersoff, J.; Reuter, M. C.; Stach, E. A.; Ross, F. M. Step-Flow Kinetics in Nanowire Growth. *Phys. Rev. Lett.* 2010, 105, (19), 195502, DOI: 10.1103/PhysRevLett.105.195502
18. Chou, Y.-C.; Wen, C.-Y.; Reuter, M. C.; Su, D.; Stach, E. A.; Ross, F. M. Controlling the Growth of Si/Ge Nanowires and Heterojunctions Using Silver–Gold Alloy Catalysts. *ACS Nano* 2012, 6, (7), 6407-6415, DOI: 10.1021/nn301978x
19. Maksimova, K. Y.; Kozlov, A. A.; Shvets, P. V.; Koneva, U. Y.; Yurkevich, O. V.; Lebedev, O. I.; Vyvenko, O. F.; Mikhailovskii, V. Y.; Goikhman, A. Y. Copper-Stabilized Si/Au Nanowhiskers for Advanced Nanoelectronic Applications. *ACS Omega* 2018, 3, (2), 1684-1688, DOI: 10.1021/acsomega.7b01640
20. Lugstein, A.; Steinmair, M.; Hyun, Y. J.; Bertagnolli, E.; Pongratz, P. Ga/Au alloy catalyst for single crystal silicon-nanowire epitaxy. *Appl. Phys. Lett.* 2007, 90, (2), 023109, DOI: 10.1063/1.2431468
21. Yu, Z.; Lu, J.; Qian, S.; Misra, S.; Yu, L.; Xu, J.; Xu, L.; Wang, J.; Shi, Y.; Chen, K.; Roca i Cabarrocas, P. Bi-Sn alloy catalyst for simultaneous morphology and doping control of silicon nanowires in radial junction solar cells. *Appl. Phys. Lett.* 2015, 107, (16), 163105, DOI: 10.1063/1.4933274
22. Tang, J.; Maurice, J. L.; Fossard, F.; Florea, I.; Chen, W.; Johnson, E. V.; Foldyna, M.; Yu, L.; Roca i Cabarrocas, P. Natural occurrence of the diamond hexagonal structure in silicon nanowires grown by a plasma-assisted vapour–liquid–solid method. *Nanoscale* 2017, 9, (24), 8113-8118, DOI: 10.1039/C7NR01299C

23. Wang, W. Plasma-enhanced CVD growth of cubic and hexagonal diamond silicon nanowires with liquid-solid mixed catalysts for photovoltaic applications. PhD thesis, Institut Polytechnique de Paris, École polytechnique, 2021.
24. Fan, Z.; Maurice, J.-L.; Chen, W.; Guilet, S.; Cambril, E.; Lafosse, X.; Couraud, L.; Merghem, K.; Yu, L.; Bouchoule, S.; Roca i Cabarrocas, P. On the Mechanism of In Nanoparticle Formation by Exposing ITO Thin Films to Hydrogen Plasmas. *Langmuir* 2017, 33, (43), 12114-12119, DOI: 10.1021/acs.langmuir.7b01743
25. Fürtauer, S.; Li, D.; Cupid, D.; Flandorfer, H. The Cu–Sn phase diagram, Part I: New experimental results. *Intermetallics* 2013, 34, 142-147, DOI: 10.1016/j.intermet.2012.10.004
26. Stadelmann, P. A. EMS - a software package for electron diffraction analysis and HREM image simulation in materials science. *Ultramicroscopy* 1987, 21, (2), 131-145, DOI: 10.1016/0304-3991(87)90080-5
27. Stadelmann, P. JEMS-Swiss. <https://www.jems-swiss.ch/>
28. Wen, C. Y.; Spaepen, F. In situ electron microscopy of the phases of Cu<sub>3</sub>Si. *Philos. Mag.* 2007, 87, (35), 5581-5599, DOI: 10.1080/14786430701675829
29. Arbiol, J.; Kalache, B.; Roca i Cabarrocas, P.; Morante, J. R.; Fontcuberta i Morral, A. Influence of Cu as a catalyst on the properties of silicon nanowires synthesized by the vapour–solid–solid mechanism. *Nanotechnology* 2007, 18, (30), 305606, DOI: 10.1088/0957-4484/18/30/305606
30. Yao, Y.; Fan, S. Si nanowires synthesized with Cu catalyst. *Mater. Lett.* 2007, 61, (1), 177-181, DOI: 10.1016/j.matlet.2006.04.045
31. Renard, V. T.; Jublot, M.; Gergaud, P.; Cherns, P.; Rouchon, D.; Chabli, A.; Jousseume, V. Catalyst preparation for CMOS-compatible silicon nanowire synthesis. *Nature Nanotech.* 2009, 4, (10), 654-657, DOI: 10.1038/nnano.2009.234
32. Wen, C. Y.; Reuter, M. C.; Tersoff, J.; Stach, E. A.; Ross, F. M. Structure, Growth Kinetics, and Ledge Flow during Vapor–Solid–Solid Growth of Copper-Catalyzed Silicon Nanowires. *Nano. Lett.* 2010, 10, (2), 514-519, DOI: 10.1021/nl903362y
33. Istratov, A. A.; Flink, C.; Hieslmair, H.; Weber, E. R.; Heiser, T. Intrinsic Diffusion Coefficient of Interstitial Copper in Silicon. *Phys. Rev. Lett.* 1998, 81, (6), 1243-1246, DOI: 10.1103/PhysRevLett.81.1243
34. Bracht, H. Copper related diffusion phenomena in germanium and silicon. *Mater. Sci. Semicond. Process.* 2004, 7, (3), 113-124, DOI: 10.1016/j.mssp.2004.06.001
35. Wen, C. Y.; Tersoff, J.; Hillerich, K.; Reuter, M. C.; Park, J. H.; Kodambaka, S.; Stach, E. A.; Ross, F. M. Periodically Changing Morphology of the Growth Interface in Si, Ge, and GaP Nanowires. *Phys. Rev. Lett.* 2011, 107, (2), 025503, DOI: 10.1103/PhysRevLett.107.025503
36. Olesinski, R. W.; Abbaschian, G. J. The Si–Sn (Silicon–Tin) system. *Bull. Alloy Phase Diag.* 1984, 5, (3), 273-276, DOI: 10.1007/BF02868552

37. Olesinski, R. W.; Abbaschian, G. J. The Cu–Si (Copper-Silicon) system. *Bull. Alloy Phase Diag.* **1986**, 7, (2), 170-178, DOI: 10.1007/BF02881559
38. Hofmann, S.; Sharma, R.; Wirth, C. T.; Cervantes-Sodi, F.; Ducati, C.; Kasama, T.; Dunin-Borkowski, R. E.; Drucker, J.; Bennett, P.; Robertson, J. Ledge-flow-controlled catalyst interface dynamics during Si nanowire growth. *Nature Mater.* **2008**, 7, (5), 372-375, DOI: 10.1038/nmat2140
39. Cui, H.; Lü, Y. Y.; Yang, G. W.; Chen, Y. M.; Wang, C. X. Step-Flow Kinetics Model for the Vapor–Solid–Solid Si Nanowires Growth. *Nano. Lett.* **2015**, 15, (5), 3640-3645, DOI: 10.1021/acs.nanolett.5b01442
40. Nguyen, P.; Ng, H. T.; Meyyappan, M. Catalyst Metal Selection for Synthesis of Inorganic Nanowires. *Adv. Mater.* **2005**, 17, (14), 1773-1777, DOI: 10.1002/adma.200401717
41. Kallesøe, C.; Wen, C.-Y.; Mølhave, K.; Bøggild, P.; Ross, F. M. Measurement of Local Si-Nanowire Growth Kinetics Using In situ Transmission Electron Microscopy of Heated Cantilevers. *Small* **2010**, 6, (18), 2058-2064, DOI: 10.1002/smll.200902187
42. Panciera, F.; Norton, M. M.; Alam, S. B.; Hofmann, S.; Mølhave, K.; Ross, F. M. Controlling nanowire growth through electric field-induced deformation of the catalyst droplet. *Nat. Commun.* **2016**, 7, 12271, DOI: 10.1038/ncomms12271

## BRIEFS

*In situ* transmission electron microscopy unravels a surprising step-flow motion during the growth of Si nanowires with dual-phase liquid-solid Sn-Cu catalysts.

## SYNOPSIS

